Mon. Not. R. Astron. Soc. **000**, 000–000 (0000) Printed 2 September 2011 (MN LATEX style file v2.2)

Exploring the dust content of SDSS DR7 damped Lyman alpha systems at 2.15$\leqslant z_{ab} <$5.2

Pushpa Khare[1⋆], Daniel Vanden Berk[2], Donald G. York[3,4], Britt Lundgren[5] , Varsha P. Kulkarni[6]
[1]*CSIR Emeritus Scientist, IUCAA, Ganeshkhind, Pune, 411007, India*
[2]*Physics Department, St. Vincent College, Latrobe, PA 15650, USA*
[3]*Department of Astronomy and Astrophysics, University of Chicago, Chicago, IL 60637, USA*
[4]*Enrico Fermi Institute, University of Chicago, Chicago, IL 60637, USA*
[5] *Department of Astronomy, Yale University, New Haven, CT 06520-8101, USA*
[6] *Department of Physics and Astronomy, University of South Carolina, Columbia, SC 29208, USA*

ABSTRACT
We have studied a sample of 1084 intervening absorption systems with 2.15$\leqslant z_{ab} \leqslant$5.2, having log($N_{HI}$) $>$ 20.0 in the spectra of QSOs in Sloan Digital Sky Survey (SDSS) data release 7 (DR7), with the aim of understanding the nature and abundance of the dust and the chemical abundances in the DLA absorbers. Composite spectra were constructed for the full sample and several subsamples, chosen on the basis of absorber and QSO properties. Average extinction curves were obtained for the samples by comparing their geometric mean composite spectra with those of two samples of QSOs, matching in z_{em} and i magnitude with the DLA sample, one sample without any absorbers along their lines of sight and the other without any DLAs along their lines of sight irrespective of the presence of other absorption systems. We also derived relative extinction curves of several pairs of subsamples. While the average reddening in the DLA sample is small, we find definite evidence for the presence of dust in subsamples based on absorber properties, in particular the strength of metal absorption lines. DLAs along lines of sight to QSOs which are not colour selected are found to be more dusty compared to those along the lines of sight to the more numerous colour selected QSOs. From these studies and from the strengths of absorption lines in the composite spectra, we conclude that $\leqslant$ 10% of the DLAs in SDSS DR7 cause significant reddening, have stronger absorption lines and have higher abundances as compared to the rest of the sample. The rest of the sample shows little reddening. While due to the dominant color selection method used to target QSOs in the SDSS DR7, this fraction of 10% likely represents a lower limit for the global fraction of dusty DLAs at high-z, it is also possible that the dust grain sizes at high redshifts are larger, giving rise to a flat extinction curve over the observed range of wavelengths.

Key words: Quasars: absorption lines-ISM: abundances, dust, extinction-Galaxies: high-redshift

1 INTRODUCTION

Early attempts to quantitatively detect dust in damped Lyman alpha absorbers in QSO spectra, by its differential extinction of a given object, were made by Pei, Fall & Bechtold (1991). They found higher extinction in a sample of 13 QSOs having damped Ly α systems (DLAs) in their spectra compared to a sample of 15 QSOs that had no DLAs indicating presence of dust in the DLA absorbers, albeit with $E(B-V)$ <0.03. Ellison, Hall & Lira (2005) similarly found only a slight reddening ($E(B-V) <$ 0.04) in 14 out of 42 QSOs with DLAs.

The Sloan Digital Sky Survey (SDSS) archive has been used for several studies of extinction in sight-lines to QSOs. Richards et al. (2003) showed that an observer frame colour excess, hereafter, $\Delta(g-i)$, which is the difference between the actual colours of a QSO and the median colours of QSOs at that redshift, could be defined for the SDSS QSO spectra and could be used to form templates of objects with apparent degrees of extinction. However, they could not discern if the extinction so detected was from the QSO itself or from intervening systems. Hopkins et al. (2004) used composite QSO spectra to show that the extinction towards QSOs is dominated by SMC-like extinction, which they argued was predominantly located at QSO redshifts. Wild & Hewett (2005) have found evidence of dust in QSO absorption line systems with de-

⋆ E-mail: pushpakhare@gmail.com

tected Ca II lines, with $E(B-V)$ of 0.06. Wild, Hewitt & Pettini (2005) find strong Ca II absorbers to have $E(B-V) > 0.1$. However, these samples are small and highly selective. Nestor et al. (2008) find no evidence that $N_{\rm CaII}$ in DLAs is related to the presence of dust depletion of Cr. Murphy & Liske (2004) studied the spectral indices of QSOs in SDSS Data Release 2 and found no evidence for the presence of dust in DLAs at a redshift ~ 3. They derived an upper limit of 0.02 on $E(B-V)$.

York et al. (2006; hereafter Y06) gave definite evidence of dust in the intervening Mg II absorbers by comparing composite spectra of SDSS QSOs with absorbers with that of a matching (in z_{em} and i magnitude (m_i)) sample (the non-absorber sample) of SDSS QSOs without any absorbers in their spectra. The reddening was shown to be correlated with several absorber properties, in particular the strength of Mg II lines (essentially, the velocity spread of multiple, saturated components). Vanden Berk et al. (2008), using the method of Y06, similarly obtained evidence for reddening in systems associated with QSOs (having relative velocity with respect to the QSO smaller than 3000 km s^{-1}). Ménard et al. (2008), investigated the effect of dust reddening and gravitational lensing of Mg II absorbers in SDSS DR4 QSOs and derived the dependence of reddening on redshift and on Mg II equivalent width.

Recently, Frank and Péroux (2010; hereafter FP10) used the method of Y06 to study the dust content in intervening DLAs at redshifts of > 2.2. They found no evidence of dust in their sample of 731 DLAs and subsamples there of. This result is surprising in view of the fact that several of the high $N_{\rm HI}$ systems at $1.8 < z_{ab} < 4.2$ have been found to have molecular hydrogen which appears to be associated with significant depletion of Fe (Noterdaeme et al. 2008). Molecular hydrogen is believed to form on the surface of dust grains (Hollenbach & Salpeter 1970) and depletion of Fe is thought to be related, in some cases, to gas phase depletion onto solid particles. The result of FP10 thus prompted us to further investigate the dust content of DLAs. We do note that Tumlinson et al. (2002) have found modest amounts of H_2 in the LMC and the SMC along sight lines having low $E(B-V)$. Both these clouds are known to have dust properties different from those of the dust in the Milky Way.

In this paper, we present the results of our investigations. Section 2 describes our sample selection and generation of composite spectra, section 3 describes the results and conclusions are presented in section 4.

2 SAMPLE SELECTION AND GENERATION OF COMPOSITE SPECTRA

A sample of intervening absorption systems (with relative velocities with respect to QSOs > 5000 km s^{-1}) having neutral hydrogen column densities $\geqslant 10^{20}$ cm^{-2} in the SDSS DR7 has been compiled by Noterdaeme et al. (2009b). We used their sample which consists of 1426 systems at redshifts between 2.15 and 5.2.

Following FP10, we removed QSOs having more than one of these systems along the line of sight. Quasars containing likely broad absorption line systems (BALs) were removed from the sample and from the comparison sample of matched quasars (described below). All BALQSOs identified in the SDSS Data Release 5 (DR5) catalog by Gibson et al. (2009) were removed. We manually searched for BALQSOs among all of the quasars in the DR7 quasar catalog (Schneider et al. 2010) that are not also in the DR5 catalog. The number of quasars inspected is 28532. A broad absorption line system candidate was defined as any absorption feature that appeared to be at least broad enough that it could be a C IV, Mg II, or some other doublet line with heavily blended components. That is, any feature broad enough that a common absorption doublet could not be visually resolved in the spectrum was considered a candidate BAL. (We call the objects "candidate" BALs because they have not been quantitatively analyzed to determine if they meet various criteria listed in published BALQSO catalogs.) The selection procedure using this definition was simple to implement, and the results corresponded well with those in the Gibson et al. (2009) catalog. We also inspected all of the post DR5 candidate BALQSOs identified by Shen et al. (2011), using the same selection criteria. Each post DR5 BALQSO candidate was inspected by at least three people. A total of 2206 BALQSO candidates were identified, among 28532 quasars. The candidate BALQSO fraction (7.7%) in the post DR5 quasar sample is slightly larger than the BALQSO fraction (6.5%) in the Gibson et al. (2009) catalog. Thus we have likely selected somewhat more candidate BALQSOs than the Gibson et. al. procedure would have. For the purposes of this paper, the difference is minor, and it means that we are slightly less likely to include quasars with strong (non-DLA) absorption among the matched samples.

This left us with 1084 systems out of which 721 systems are classical DLAs, having $\log(N_{\rm HI}) \geqslant 20.3$ and the rest, 363 are sub-DLAs, having $\log(N_{\rm HI})$ between 20 and 20.3. These 1084 systems form our primary absorber sample S1. The redshift distribution of S1 is shown in Fig.1. It can be seen that most (93%) of the systems in S1 have redshifts between 2.25 and 4. Several subsamples constructed from S1 are listed in Table 1 which lists the selection criteria, number of systems in the samples, and average values of $N_{\rm HI}$, z_{ab} and m_i for the samples. Values of $E(B-V)$ (described below) are also given.

We also inspected the matched non-DLA sample of FP10 (matched spectrum data list sent courtesy of Stephan Frank) to check whether any BALQSOs may have been included in that sample. Of the 731 matched quasars used by FP10, there are 60 candidate BALQSOs from our combined SDSS DR7 list. In addition there are 29 DLAs which have inexplicably found their way into the matching non-DLA sample used by FP10, most of which are matches with the DLA itself. The inclusion of BALQSOs and DLA quasars in the matched quasar sample *may* explain at least in part why FP10 did not detect significant reddening associated with DLAs —the matched sample may have been artificially reddened due to the inclusion of BALQSOs which are known to be dusty and quasars with DLAs. We have therefore, repeated some of the analysis of FP10.

Below we briefly describe the method of generation and use of composite spectra as advocated by Y06. Further details can be found in Y06. To generate an arithmetic mean composite, the spectra were first normalized by reconstructions of the QSO continua, using the first 30 QSO eigenspectra derived by Yip et al. (2004). The spectra were then shifted to the absorber rest frame. The pixels flagged by the spectroscopic pipeline as possibly bad in some way (Stoughton et al. 2002) were masked and not used in constructing the composites. Also masked were pixels within 5 Å of the expected line positions of detected absorption systems unrelated to the target system. After masking pixels, the normalized flux density in each remaining pixel was weighted by the inverse of the associated variance, and the weighted arithmetic mean of all contributing spectra was calculated for each pixel.

The geometric mean of a set of power law spectra preserves the average power law index of the spectra, so it is the appropriate statistic to use to determine the characteristic extinction law (likely

Table 1. Samples: Definitions and properties

Sample	Selection Criteria	Number of systems	$E(B-V)^a$	$E(B-V)^b$	$< z_{ab} >$	log$<$N$_{\rm HI}>$	$<$m$_i>$	$< \Delta(g-i) >$
S1	Full sample	1084	0.0014	-0.0026	2.9323	20.72	18.98	-0.011
S2	m$_i^c$ $<$19.5	847	0.0046	0.0005	2.8914	20.74	18.77	-0.014
S3	m$_i$ $<$19.5,	545	0.0044^d	0.0008^d	2.8436	20.72	18.99	0.000
	$\|\Delta$ M$_i^e\|^f < 0.1$ &	799^g			2.8703	20.74	18.82	-0.001
	$\|\Delta$z$_{em}\|^f < 0.05$							
S4	m$_i$ $<$19.5,	609	0.0050	0.0007	2.8644	20.73	18.96	-0.001
	$\|\Delta$ M$_i^e\| < 0.15$ &	830^g			2.8644	20.75	18.80	0.000
	$\|\Delta$z$_{em}\| < 0.1$							
S5	log(N$_{\rm HI}$) $\geqslant 20.49$	538	0.0028	-0.0009	2.9484	20.95	18.95	-0.008
S6	log(N$_{\rm HI}$) < 20.49	546	0.0000	-0.0043	2.9164	20.25	19.01	-0.014
S7	m$_i$ $\geqslant$19.05	545	-0.0036	-0.0072	3.0814	20.69	19.47	0.002
S8	m$_i$ $<$19.05	539	0.0053	0.0008	2.7815	20.76	18.49	-0.024
S9	M$_i$ $\geqslant$-27.42	546	-0.0022	-0.0068	2.8614	20.68	19.39	0.00
S10	M$_i$ $<$-27.42	538	0.0065	0.0027	3.0042	20.76	18.57	-0.022
S11	z$_{ab}$ $\geqslant 2.89$	543	-0.0008	-0.0048	3.2943	20.75	19.14	0.014
S12	z$_{ab} < 2.89$	541	0.0025	-0.0013	2.5688	20.69	18.83	-0.036
S13	z$_{em}$ $\geqslant 3.26$	538	-0.0001	-0.0036	3.2370	20.76	19.10	0.033
S14	z$_{em} < 3.26$	546	0.0019	-0.0020	2.6320	20.69	18.86	-0.054
S15	$\Delta(g-i) \geqslant -0.01$	547	0.0110	0.0068	2.9254	20.79	18.91	-0.012
S16	$\Delta(g-i) < -0.01$	537	-0.0090	-0.0131	2.9393	20.64	19.06	-0.009
S17	W$^h_{\rm SiII}$ $\geqslant 0.62$	213	0.0058	0.0010	2.8740	20.93	19.02	-0.015
S18	W$_{\rm SiII} < 0.62$	226	0.0045	-0.0022	2.7281	20.73	18.48	-0.062
S19	log(N$_{\rm HI}$) $\geqslant 21.0$	149	0.0081	-0.0014	2.9903	21.26	18.89	0.008
S20	log(N$_{\rm HI}$) < 21.0	935	0.0004	-0.0030	2.9230	20.51	19.00	-0.014
S21	$\Delta(g-i) \geqslant 0.3$	60	0.0290	0.0290	3.1925	20.93	18.93	0.007
S22	$\Delta(g-i) < 0.3$	1024	-0.0002	-0.0045	2.9170	20.71	18.99	-0.012
S23	W$_{\rm SiII}$ $\geqslant 1.0$	106	0.0097	0.0054	2.9526	20.99	19.09	-0.009
S24	W$_{\rm SiII} < 1.0$	333	0.0039	-0.0026	2.7500	20.78	18.64	-0.049
S25	W$_{\rm SiII}$ $\geqslant 1.5$	56	0.0092	-0.0008	3.0427	21.04	19.04	-0.001
S26	W$_{\rm SiII} < 1.5$	383	0.0049	-0.0008	2.7633	20.80	18.70	-0.045

a: Extinction of the absorber sample with respect to the corresponding non-absorber sample assuming SMC extinction law
b: Extinction of the absorber sample with respect to the corresponding non-DLA sample assuming SMC extinction law
c: i magnitude corrected for Galactic extinction
d: One σ error from bootstrap analysis is $\simeq$0.0015
e: Absolute i magnitude
f: Absolute values of the difference between absorber and non-absorber QSO pairs
g: Values in this row are obtained when non-DLA sample is used as the matching sample.
h: Rest equivalent width of Si IIλ1526

to be approximated by a power law) of the absorber sample. The geometric mean composite spectrum for an absorber sample was generated by shifting the spectra to the absorber rest frames and taking their geometric mean. The non-absorber sample was compiled by selecting one non-absorber QSO (not having any absorption lines in its spectrum) for each QSO in the absorber sample, having nearly the same z$_{em}$ and M$_i$ (see Y06 for details). To generate the geometric mean of the non-absorber sample, each non-absorber spectrum was first shifted to the rest frame of the absorber in the corresponding absorber QSO. As long as the spectroscopic properties of the QSOs in the absorber and non-absorber samples are statistically equivalent (which is ensured by their having similar z$_{em}$ and M$_i$), except for the effects of the intervening absorption systems, dividing the absorber composite by the non-absorber composite will yield the relative extinction curve in the absorber frame. In doing this, the non-absorber spectrum is scaled so that the average flux densities in the reddest 100 Å of both spectra are equal. The extinction curve can be fitted with the SMC, LMC or Milky Way (MW) extinction curves to obtain the average $E(B-V)$ for the absorber sample. For generating both types of composites, we used only parts of spectra having $\lambda > 1250$ Å in the rest frame of QSOs in order to avoid any contamination by the Lyman alpha forest in the spectra.

Although FP10 use the method of composite spectra as advocated by Y06, their procedure differed from Y06 in respect of the use of the matching non-absorber sample. They used the sample of QSOs not having DLAs (non-DLA sample) as their non-absorber sample, arguing that any other (lower H I column density) systems will be found with equal probability in the absorber as well as the non-DLA sample and the effect of these systems should cancel out.

We use both types of comparison samples: one comprising of QSOs having no absorbers along the line of sight (the non-absorber sample) and the other comprising of QSOs having no DLAs along the line of sight irrespective of the presence or absence of other absorption systems (the non-DLA sample). The composite spectra of the non-absorber sample would be completely devoid of reddening due to intervening absorbers and a comparison with the composite of QSOs having DLAs along their lines of sight should reveal any weak reddening present in these QSOs. On the other hand, reddening caused by any non-DLA absorption systems would statistically

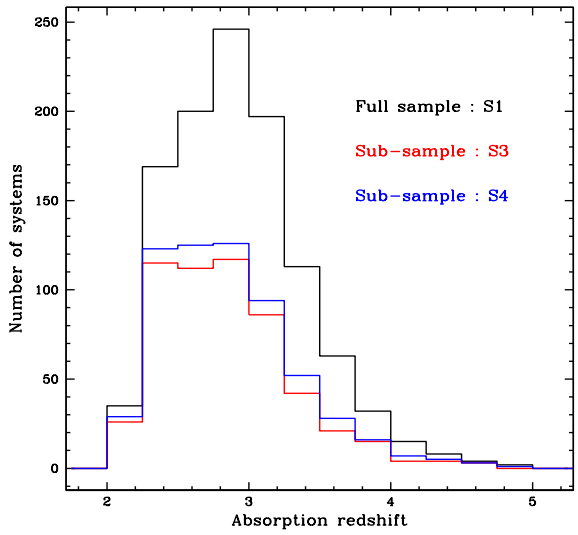

Figure 1. Histograms showing the redshift distribution of systems in samples S1, S3 and S4. About 93-94% of the systems in all three samples have redshifts between 2.25 and 4.

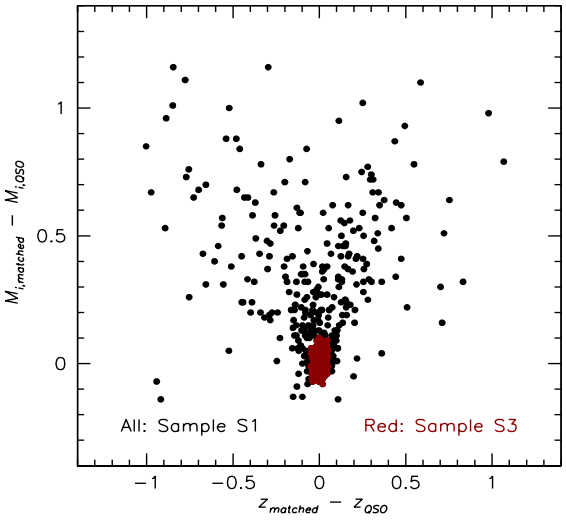

Figure 2. Plot showing the differences between z_{em} and M_i of the QSOs in the full DLA sample (S1) and the matching non-absorber sample. In some cases the differences are large, with $|\Delta z_{\rm em}|$ and $|\Delta M_{\rm i}|$ reaching up to >1. The points for QSOs in S3 are shown in red.

cancel out when the composite of absorber sample is compared with that of the matching non-DLA sample, giving an estimate of reddening due to the DLAs alone.

For compiling the matching non-absorber sample, we selected from DR7, QSOs without any absorption systems of grade A and B. We chose to ignore any grade C, D, E systems that may be present in the QSO spectra as these are not likely to produce significant reddening as noted by Y06. Details of the system grades can be found in Y06. In Fig.2 we have plotted the difference in M_i and z_{em} between the full sample S1 and the corresponding non-absorber sample. For some QSOs, differences are large, reaching up to > 1.

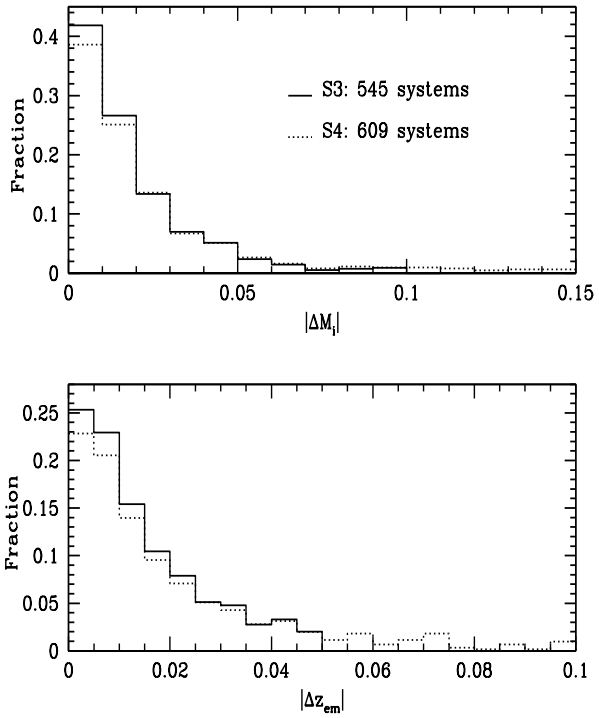

Figure 3. Histograms showing absolute values of the difference between the i magnitudes (upper panel) and emission redshifts (lower panel) of the absorber-non-absorber QSO pairs for subsamples S3 and S4.

As identification of absorption systems is difficult in the spectra of faint QSOs (which have smaller S/N) we constructed a subsample of S1 having QSOs with Galactic extinction corrected, i magnitude < 19.5 so that the S/N of the corresponding non-absorber spectra will be sufficiently high to ascertain the absence of absorption systems. This subsample of S1 (S2) has 847 systems.

The values of the differences in M_i and z_{em} of the pairs of QSOs in the absorber subsample S2 and the corresponding non-absorber sample are also as large as those for S1, and the match between M_i and z_{em} of the absorber and non-absorber QSO pairs is not as good as that obtained for the lower redshift Mg II sample of Y06 or the non-DLA-absorber sample of FP10. For better comparison of the composites, we therefore, chose two subsamples: S3 having 545 systems with $|\Delta M_i| < 0.1$ and $|\Delta z_{em}| < 0.05$ and S4 having 609 systems with $|\Delta M_i| < 0.15$ and $|\Delta z_{em}| < 0.1$. The redshift distributions for these subsamples are also shown in Fig.1. About 94% of the systems in these subsamples also have their redshifts between 2.25 and 4. The points corresponding to subsample S3 are shown in red in Fig.2. The histograms showing the distributions of $|\Delta M_i|$ and $|\Delta z_{em}|$ for these subsamples are shown in Fig.3. The values are mostly small and the subsamples can be used to get reliable estimates of reddening. We constructed the matching sample of non-DLAs in similar way. The number of non-DLAs in SDSS DR7 being very large, better matches were obtained between the parameters of the QSOs in S1 and those of the matching non-DLA QSOs, with $|\Delta z_{em}|$ and $|\Delta M_i|$ being smaller than 0.32 and 0.4 respectively.

3 RESULTS

3.1 Reddening

The composites of S1 and of the corresponding non-absorber sample, as well as the ratio of the two composites (the extinction curve for S1) are plotted in Fig.4. The best fit extinction curves for SMC as well as for the MW are plotted. Values of $E(B-V)$ are small. $E(B-V)$ does not change if we restrict the spectra to wavelengths smaller than 2400 Å. In Table 1 we give values of $E(B-V)$ with respect to both the non-absorber and non-DLA matching samples for all subsamples, assuming the SMC extinction law. Values of $E(B-V)$ for S3 and S4, using non-absorber samples, are 0.0044 and 0.0050 respectively. Formal errors are rather small and a bootstrap analysis for S3 indicates 1 σ error $\sim$ 0.0017 for both non-absorber as well as non-DLA matching samples. Thus there is weak (2-3 σ) evidence for reddening along the average DLA sight lines when compared to the non-absorber sample. Using the non-DLA matching sample gives even smaller reddening (listed in Table 1) which is expected as the reddening caused by other non-DLA absorption systems along the line of sight could cancel out.

Pettini et al. (1997) have argued that the dust to gas ratio is likely to be smaller in high redshift DLAs as compared to the MW due to their lower metal abundance, and lower depletion factors compared to that in the MW, resulting in a small amount of extinction. Following their argument, assuming the dust to gas ratio to be $1/30^{th}$ of that in the MW, and assuming $N_{HI}/E(B-V) \simeq 5\times10^{21}$ cm^{-2} for the MW (Diplas & Savage 1994), our subsamples S3 and S4 would have $E(B-V)$ of $\sim$ 0.003 in the absorber rest-frame. This is considerably larger than, but is within 2 σ of, the $E(B-V)$ obtained using the non-DLA matching sample. It is somewhat smaller than, but again within 1 σ of, the value obtained using the non-absorber matching sample. However, we note that several of the QSOs in our DLA sample should have lower redshift Mg II systems which should produce extinction as found by Y06. Their full sample of 809 Mg II systems with $W_{MgII} > 0.3$ Å has $E(B-V)$ of 0.01 which will correspond to an E(B-V) of 0.0053 in the rest frame of the present DLA sample assuming the SMC extinction law. So the $E(B-V)$ obtained using the non-absorber sample also seems to be much smaller than the expected value, albeit within 3 σ of it. Note that 0.0053 should roughly be the difference between the $E(B-V)$ values obtained using the non-absorbers and non-DLA matching samples (values in columns 4 and 5 of table 1). This seems to be true for most of the subsamples having low reddening (for which the difference of 0.0053 will be significant). So the method seems to be giving consistent results and the average reddening in the whole DLA sample appears to be very small.

We do expect some DLAs at high redshifts to have higher reddening in view of the following facts: (1) According to Noterdaeme et al. (2008) at least 16% of the DLAs (having log(N_{HI}) > 20) at high redshifts have molecular hydrogen and there is a strong preference of H_2 bearing DLAs to have significant depletion factors, 0.95>[X/Fe]>0.3, which could indicate significant amount of dust in these systems. A correlation between molecular hydrogen column density and colour excess is seen in the MW clouds (Rachford et al. 2002) for $E(B-V) < 0.1$. (2) Some of the DLAs at high redshifts have been found to have depletion patterns similar to those in the MW (Srianand et al. 2008), indicating the presence of dust similar to that in cold ISM of the Galaxy. (3) DLAs at redshift > 1.5 have been found to exhibit the 2175 Å bump (e.g. Noterdaeme et al. 2009a; Jiang et al. 2010) which again indicates the presence of MW type dust in these absorbers. (4) A DLA at redshift of 2.45 in a GRB has the 2175 Å bump in its rest frame (Eliasdottir et al. 2009).

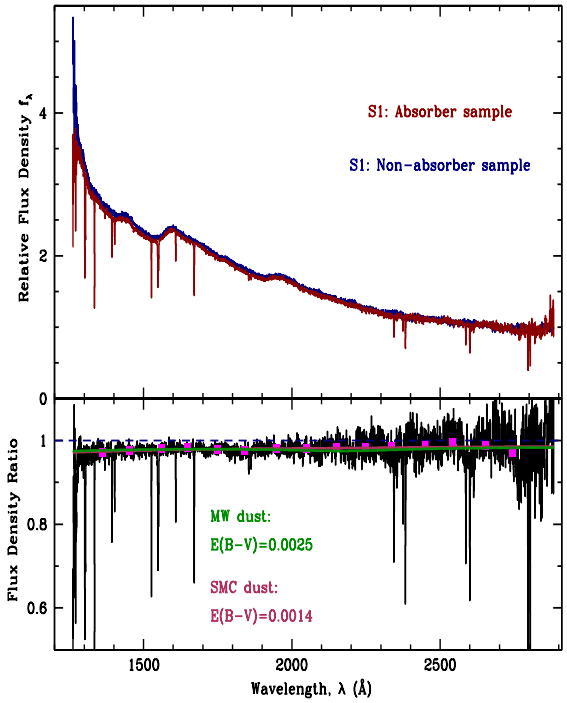

Figure 4. The top panel shows the composite spectrum (geometric mean) of the absorbers in subsample S1, in their rest-frames, in red, and that of the corresponding non-absorbers, in blue. The two spectra have been normalized at the higher wavelength end. The bottom panel shows the ratio of the two spectra along with the best fit SMC extinction curve in red and MW extinction curve in green. Pink squares are average flux density ratios over 100 Å bands, plotted to guide the eye.

3.1.1 *Distribution of* $\Delta(g-i)$

To explore the issue of dust in DLAs further, we looked at the distributions of the $\Delta(g-i)$ values of the absorber and the non-absorber sample. These are shown in Fig.5a for subsample S3. The distributions do appear to be different. The mean, sigma and median values for the absorber and the non-absorber samples are given in Table 2. Similar values are also given for S4. The 1 σ error on the difference in the mean values of $\Delta(g-i)$ is $\sim$ 0.012.Thus the $\Delta(g-i)$ values of the absorber and non-absorber samples differ at 6 σ level. The Kolmogorov-Smirnov (KS) probabilities for the distributions of $\Delta(g-i)$ for the absorber and non-absorber samples to be similar is close to zero for both S3 and S4. We note that the KS test compares the shapes of distributions of the $\Delta(g-i)$ values of the absorber and the non-absorber sample rather than comparing their average or median values, and gives the probability for the two distributions being drawn from a parent distribution. We have also plotted in Fig.5a the $\Delta(g-i)$ distribution for the 9768 DR7 QSOs having $z_{em} > 2.2$ and $m_i < 19.5$. Values of the mean and variance for this sample are also included in Table 2. The mean values are different at high significance level from those for the absorber as well as the non-absorber sample. The KS probability for the distribution of $\Delta(g-i)$ in DR7 plotted in the figure and the absorber subsamples S3 and S4 as well as corresponding non-absorber sam-

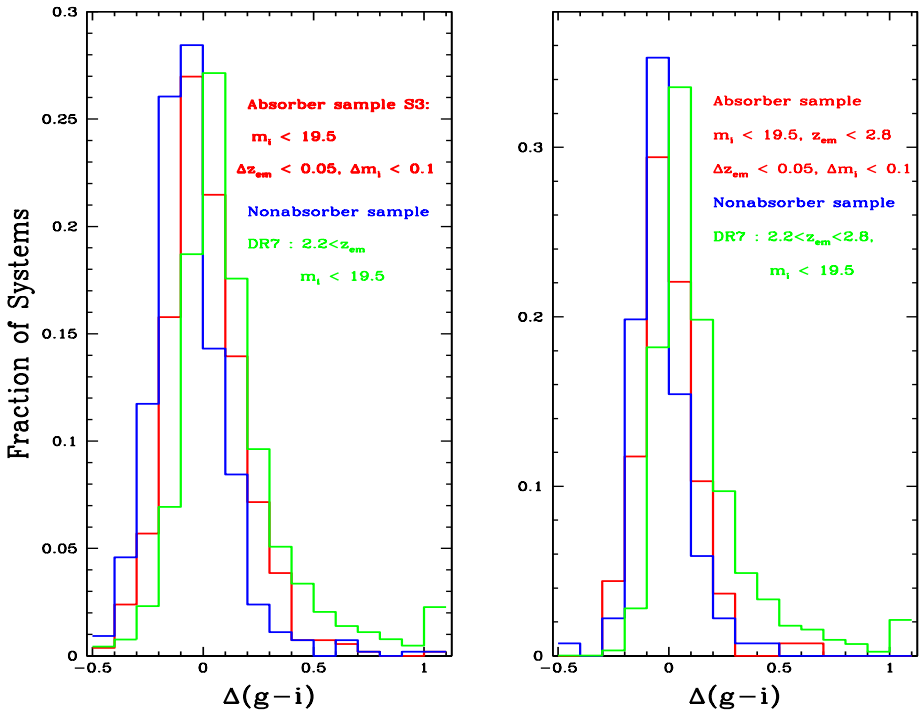

Figure 5. (a; left panel) The figure shows the histogram, in red, of observer frame colour excess $\Delta(g-i)$ for the subsample S3. The distribution for corresponding non-absorber sample is shown in blue. The green histogram shows the distribution for 9768 QSOs in DR7 having galactic extinction corrected i magnitude smaller than 19.5 and having $z_{em} > 2.2$. (b; right panel) The plots in this panel are similar except that only QSOs with $2.8 > z_{em} > 2.2$ are included in all the three samples. There are 5378 DR7 QSOs in this plot.

Table 2. Mean and median values of $\Delta(g-i)$ for various subsamples

Sample	Absorber subsample			Non-absorber sample			DR7 subsample[a]		
	Mean	Sigma	median	Mean	Sigma	median	Mean	Sigma	median
S3	0.02	0.20	-0.001	-0.058	0.19	-0.075	0.14	0.31	0.075
S4	0.02	0.22	0.000	-0.058	0.20	-0.076			
S3[b]	0.00	0.14	-0.009	-0.032	0.12	-0.042	0.16	0.29	0.085

a: DR7 QSOs having $m_i < 19.5$ and $2.2 < z_{em} < 5.2$
b: Values in this row are for systems with $z_{em} < 2.8$

Table 3. Relative reddening between subsamples

Sample A		Sample B		$E(B-V)$[a]		
Subsample	Criterion	Subsample	Criterion	SMC	LMC	MW
S5	$\log(N_{HI}) \geqslant 20.49$	S6	$\log(N_{HI}) < 20.49$	0.000	-0.002	-0.003
S7	$m_i \geqslant 19.05$	S8	$m_i < 19.05$	0.004	0.025	0.044
S9	$M_i \geqslant -27.42$	S10	$M_i < -27.42$	-0.006	0.001	0.020
S11	$z_{ab} \geqslant 2.89$	S12	$z_{ab} < 2.89$	-0.000	-0.024	-0.036
S13	$z_{em} \geqslant 3.26$	S14	$z_{em} < 3.26$	0.009	0.020	0.018
S15	$\Delta(g-i) \geqslant -0.01$	S16	$\Delta(g-i) < -0.01$	0.018	0.031	-0.006
S17	$W_{SiII} \geqslant 0.62$	S18	$W_{SiII} < 0.62$	0.006	0.021	0.015
S19	$\log(N_{HI}) \geqslant 21.0$	S20	$\log(N_{HI}) < 21.0$	0.006	-0.001	-0.017
S21	$\Delta(g-i) \geqslant 0.30$	S22	$\Delta(g-i) < 0.30$	0.038	0.069	0.010
S23	$W_{SiII} \geqslant 1.0$	S24	$W_{SiII} < 1.0$	0.008	0.019	0.006
S25	$W_{SiII} \geqslant 1.5$	S26	$W_{SiII} < 1.5$	0.006	0.015	0.009
S22	$\Delta(g-i) < 0.30$	S16	$\Delta(g-i) < -0.01$	0.007	0.013	0.000

[a] Relative extinction of subsample A with respect to subsample B

ples to be similar is also close to 0. This could partly be due to the presence of BALQSOs in the DR7 sample as seen from the high $\Delta(g-i)$ tail of the green histogram in Fig.5a and Fig.5b.

The KS test shows that the $\Delta(g-i)$ distributions of the absorber and non-absorbers samples are different. Those distributions are also different than the distributions of intermediate redshift Mg II systems described by Y06; there is a clear difference between Fig.5a and the Fig.3 of Y06. In the former, the red tail towards the high $\Delta(g-i)$ is clearly missing. It may, however, be noted that the $(g-i)$ colour loses its meaning for QSOs with $z_{em} > 2.8$ as for these QSOs, the g band falls in Lyman alpha forest and can be dictated by fluctuations from object to object in the total attenuation in the Lyman alpha forest. Only 136 out Of the 847 QSOs in S2 have emission redshifts smaller than 2.8. Thus comparison between $\Delta(g-i)$ values for the absorber and non-absorber samples may not be very meaningful as indicators of dust content of the absorbers. In Fig.5b we have plotted $\Delta(g-i)$ distributions for the three samples as in Fig.5a, restricting to QSOs having $z_{em} < 2.8$. The statistical details for these samples are included in the last row of Table 2. The mean and median values for the absorber and non-absorber samples now differ at 2 σ level and the KS probability for the distributions of $\Delta(g-i)$ for the absorber and non-absorber samples to be similar is 0.07 indicating smaller difference in the distributions of spectral shapes for the absorber and non-absorber samples. The KS probabilities for the $\Delta(g-i)$ distributions of the 5378 DR7 QSOs (having z_{em} between 2.2 and 2.8 and $m_i < 19.5$) and those of the absorber and non-absorber samples, plotted in Fig.5b, to be similar are still close to zero.

In Fig.6, we have plotted $\Delta(g-i)$ vs. N_{HI} for the entire sample S1. There does exist a weak correlation between the two quantities which could result due to the fact that stronger Lyman alpha lines, which lie in the g band for most (84%) of the QSOs (with $z_{em} > 2.8$), will result in higher g magnitudes. The slope of the best fit line drawn in the figure, is 0.103. Restricting to the 136 QSOs with $z_{em} < 2.8$, the correlation is much weaker, the slope of the best fit line being 0.027. This lends support to the above argument. In this figure we have indicated the QSOs which have not been colour selected but have been selected based on their detection in the radio or X-ray bands or have been discovered serendipitously. The best fit line for these is flatter and has a slope of 0.042. The slope of bestfit line for purely colour selected QSOs (0.107) is very close to that for the full sample S1. The KS test shows that the probability that the $\Delta(g-i)$ distribution for the colour selected and rest of the QSOs in S1 to be same is 0.2.

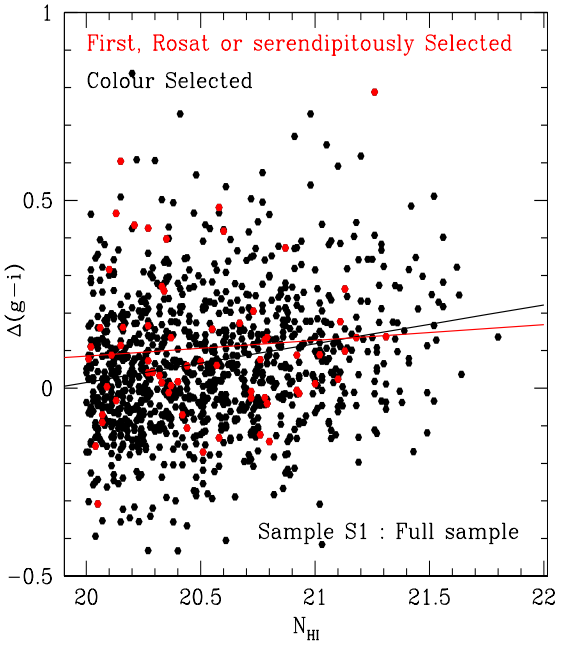

Figure 6. Plot showing observer frame colour excess $\Delta(g-i)$ as a function of H I column density in individual DLAs in S1. QSOs not selected on the basis of colours but selected on the basis of having been detected in FIRST or ROSAT survey or detected serendipitously are shown in red. The weak correlation for the full sample (slope of best fit line = 0.103) is possibly due to the fact that systems having higher H I may increase the g-magnitudes more due to their stronger Lyman α lines which lie in the g band for QSOs with $z_{em} > 2.8$. These QSOs form 87% of sample S1. For the remaining 13% of QSOs with $z_{em} \leqslant 2.8$ the best fit line is flatter having a slope of 0.027. Red line is the bestfit line for the red points and is flatter (slope 0.042) than the black line.

3.1.2 *Dependence on QSO and absorber properties*

To explore the issue of reddening further we tried to study the dependence of the slope of the composite spectra on the absorber and QSO properties. We divided the absorber sample in two roughly equal halves (see Table 1) depending on N_{HI}, z_{em}, z_{ab}, m_i, M_i, $\Delta(g-i)$ and W_{SiII} (rest equivalent width of the Si II λ1526) (subsamples S5-S18). Over the redshift range covered by our DLA sample, Mg II doublets fall outside the SDSS spectra in most cases and the most convenient lines to use as surrogates of Mg II selection are Si II λ1526 and Al II λ1670. Even though these lines are expected to be weaker than the Mg II doublet lines, they are still near saturation. We also constructed a few subsamples with different limiting values of N_{HI}, $\Delta(g-i)$, and W_{SiII} (subsamples S19-S26). The $E(B-V)$ values in Table 1 show that the reddening is higher for subsamples with (i) higher N_{HI}, (ii) fainter QSOs, (iii) lower z_{ab}, (iv) higher W_{SiII} and (v) higher $\Delta(g-i)$. We have also confirmed that the conclusions for subsamples based on the equivalent widths of Si IIλ1526 also hold for subsamples based on the equivalent widths of Al IIλ1670.

In Fig.7, we have plotted the composites of five sets of subsamples together. The spectra are normalized at the long wavelength end. It can be seen that the slope of the composite indeed depends on the absorber properties. Subsamples based on W_{SiII} and $\Delta(g-i)$ show definite relative reddening. We also constructed relative extinction curves for pairs of subsamples by dividing the composite spectrum of one subsample with that of another. Best fit values of $E(B-V)$ for all three types of extinction curves, SMC, LMC and MW, are given in Table 3. The three values for given pairs of subsamples are different. The quality of fit in the three cases is similar, SMC giving the smallest χ^2 values in most cases. Most of the $E(B-V)$ values are small. We conclude that though the reddening is not large, there is definite signature of reddening for subsamples divided with respect to N_{HI}, W_{SiII} and $\Delta(g-i)$. We further discuss this below.

3.1.3 *Dependence on the mode of selection of SDSS QSOs*

We studied the dependence of the dust content of the DLAs on the mode of selection of SDSS QSO targets. It has been argued that dusty QSOs might be missed due to the process of colour selection of targets in SDSS QSO survey (Ménard et al. 2008). In sample S1, 65 QSOs have not been selected on the basis of their colours but

have been selected on the basis of their radio or X-ray properties or have been serendipitously detected. We have constructed composite of this sample (NCS65 sample) and also of the sample of the rest of the 1019 colour selected QSOs (CS1019 sample) in sample S1. The relative $E(B-V)$ of the NCS65 with respect to CS1019 is 0.0027. The emission redshift distributions of these two samples are however different, KS test giving the probability that the two sets of redshifts to be drawn from the same distribution close to zero, the CS1019 sample having higher redshifts. Thus the relative reddening could partly be due to the difference in emission redshifts of the two samples (e.g. see samples 13 and 14 in tables 1 and 3). We therefore selected QSOs from the colour selected sample of 1019 systems (CS1019) which have z_{em} and m_i values close to those of the QSOs in the sample which were not colour selected (NCS65), using the procedure described in section 2. This new sample of 65 colour selected QSOs (CS65) has similar distribution of z_{em} and m_i as that for the sample of QSOs which are not colour selected (NCS65), KS test yielding the probability for the distributions to be same to be > 0.93. The relative $E(B-V)$ of NCS65 with respect to CS65 is 0.0020. So the QSOs selected by methods other than colour selection appear to be more reddened as compared to the colour selected QSOs. We have plotted composites for CS65 and NCS65 in the bottom panel of Fig.7. We note that only 4 systems are common in NCS65 and S23.

3.2 Line strengths

We next studied the absorption lines in the composite spectra in order to examine any correlation with absorber and QSO properties. The arithmetic mean composite of the sample S1 is shown in Fig.8. The equivalent widths of absorption lines for this spectrum are given in Table 4. The table also includes equivalent widths of the sample 1 (full sample) of Y06. The DLA systems appear to have lower ionization compared to the full sample of Y06 as seen from the considerably lower equivalent widths of C IV and Al III lines.

In order to study the dependence of line strengths on the absorber and QSO properties we have plotted in Fig.9 lines of several species for some of the subsamples from Table 1. Lines for two subsamples (in red and in black) are plotted in each row; the details of the subsamples are given in the last column of that row. Also plotted in green, are the 1 σ errors in flux of the composite spectra. As expected, lines of higher ionization are somewhat weaker and those of lower ionization are somewhat stronger in the subsample having higher H I column density. Subsample S11 with higher z_{ab} seems to have somewhat weaker lines of higher ionization species as compared to the corresponding subsample S12 at lower redshift. The difference is not very significant for Si IV lines. The difference is not likely to be due to the slight difference in the average H I column densities in these subsamples. If true this may indicate a change in the ionizing radiation.

Line strengths do seem to depend on the limiting values of $\Delta(g-i)$ and more strongly on $W_{\rm SiII}$ as seen from the 5^{th} and 6^{th} rows in Fig.9. In the third from bottom panel of the figure we have compared lines for subsamples S16 and S22. The equivalent widths of lines of subsamples having $\Delta(g-i) < -0.01$ (S16) and $\Delta(g-i) < 0.3$ (S22) are very similar. The relative $E(B-V)$ between these two subsamples is 0.007 (see Table 3). This indicates that the systems with $\Delta(g-i) < 0.3$ are basically all similar and it is only a few systems with $\Delta(g-i) \geqslant 0.3$ that have larger equivalent widths and also higher H I column densities (see Table 1). Only 13 systems are common between samples S21 and S23. Removing these systems from S21 makes the line strengths the same as those for S22 (indicating that the higher $\Delta(g-i)$ in rest of the systems in S21 may not originate in the intervening absorbers and could be intrinsic to the quasar), while removing these systems from S23 still leaves lines significantly stronger than those for S24. Thus we conclude that the line strengths are most sensitive to $W_{\rm SiII}$. S23 forms $\sim 10\%$ of the DLA sample. Some of these could be the dusty, high abundance systems found at high redshifts as mentioned in section 3.1. In the second from bottom panel of the figure we have compared lines for subsamples S19 and S23. Lines of S23 seem to be stronger than those for S19.

In the bottom panel of Fig.9, we have plotted lines for the sample of QSOs based on colour selection and not based on colour selection (NCS65 and CS65 as described in section 3.1.3). Lines of C and Al are weaker in the colour selected sample, those of Si are of similar strength, while all lines of Fe II (only one of which is included in Fig.9) are stronger in this sample. The lines O I$\lambda1302$ and Si II$\lambda1304$ are exceptionally weak in CS65 which can not be real in view of the strength of Si II$\lambda1526$ line. We believe this may be caused by the fact that the samples are small and for almost half of the samples these lines lie in the Lyman alpha forest and thus may be severely affected. The average $N_{\rm HI}$ of both samples differ by only ~ 0.1 dex. The composite spectra thus may indicate lower abundances in the colour selected sample and higher depletion of Fe and possibly Si in the sample not selected on the basis of colour. This is consistent with higher dust content of the DLAs along lines of sight to QSOs which are not colour selected.

3.3 Abundances

For the weakest lines in the composite spectrum, the least affected by saturation, the equivalent widths in the full Y06 sample and those of S1 are nearly the same (see Table 4), implying the typical column densities are similar (to within factors of 2) while the average column density of $N_{\rm HI}$ differs by a factor of 5 ($\log <N_{\rm HI}> = 20.72$ for S1 and equals 20.00 for the full sample of Y06). Evidently, all of the involved species (Si II, Zn II, Cr II, Fe II, Mn II) are more deficient compared to H I in the sample S1 of this paper. The composite spectrum thus implies lower abundance of heavy elements, in general, at high redshifts than at lower redshifts in the regions probed by QSO absorption systems. In Table 5 we have given the abundances obtained from weakest lines of the species mentioned above, assuming them to be on the linear part of the curve of growth. The abundances are about 4% of the solar values, with Fe and Mn having somewhat lower abundances. The abundances are consistent with the predictions of chemical evolution model of Pei et al. (1999). We however, note that these values are obtained from single lines and may not be robust.

As noted above, the composite spectrum for subsample S23 shows stronger lines compared to those of all other subsamples, including subsample S5 ($\log(N_{\rm HI}) \geqslant 20.48$) which has the same average H I column density and compared to those of subsample S19 which has almost twice the H I column density of as that for S23. This is also true for few other weak lines which are seen in the spectrum, namely, Al III$\lambda\lambda$ 1862 and Ni II λ1741. Thus it appears that the average abundance of S23 is higher than the rest of the sample. As noted above, the abundances of elements other than Fe seem to be lower in DLAs along the lines of sight of colour selected QSOs.

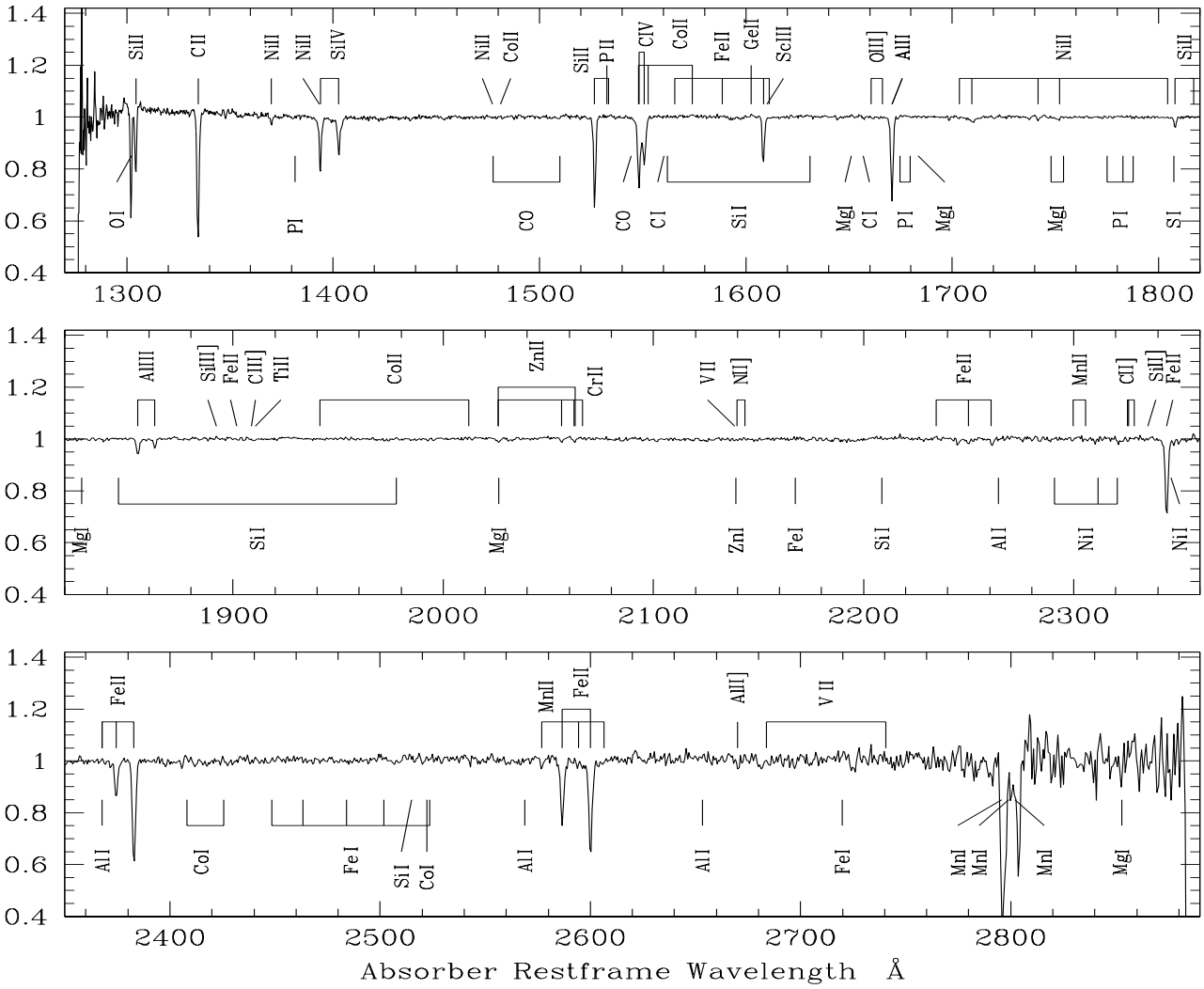

Figure 8. The arithmetic mean composite spectrum of the systems in the full sample (S1) in the absorber rest frame. The equivalent widths of the absorption lines are given in Table 4.

4 CONCLUSIONS

We have used the method of composite spectra to investigate the dust content of DLAs in the SDSS DR7 QSOs. We find definite evidence of dust, the reddening depending most sensitively on the equivalent width of Si IIλ1526 and Al IIλ1670 lines and as expected the $\Delta(g-i)$ values. The spectra of 80% of QSOs having high (>0.3) values of $\Delta(g-i)$ appear to be reddened intrinsically to the QSOs. The average differential extinction in DLA systems appears to be very small. We also compared the strengths of absorption lines in the composite spectra of different subsamples. The lines are strongest for the subsample with values of $W_{SiII} > 1.0$. Based on these studies, we conclude that $\leqslant$10% of the DLAs in our sample have significant amount of dust, and have higher abundances as compared to the rest of the sample.

The reason for the difference between the dust content of Mg II samples investigated by Y06 and the DLA sample studied in this paper could possibly be the difference in the Mg II equivalent widths and redshifts of the two samples. Mg II λ2796 is covered in only 22 of the SDSS spectra of the DLA sample, so we are unable to get meaningful value of the average equivalent width. The average redshift of S3 is 2.84 (Table 1). From Table 1 of Y06 we see that their full sample, sample 1, has an average redshift of 1.33 and $E(B-V)$ of 0.01. Assuming that the redshift dependence of absorber restframe $E(B-V)$ derived by Ménard et al. (2008) namely, $E(B-V) \propto (1+z_{ab})^{-1.1}$ for $z_{ab} < 2$ is valid at higher redshifts, sample S3 (assuming it has similar average Mg II equivalent width) can be expected to have $E(B-V)$ of $\sim$ 0.006 which is higher than the $E(B-V)$ obtained for the full sample.

As found here, most DLAs do not have significant amount of dust while 10% of the observed DLAs do have some dust and likely higher abundances. Some of these could be the dusty systems found by Srianand et al. (2008). It is possible that there is a bimodal distribution of dust in DLAs as was pointed out by Khare et al. (2007): there may be systems with much higher dust content and QSOs behind such dusty systems are too faint to be seen in

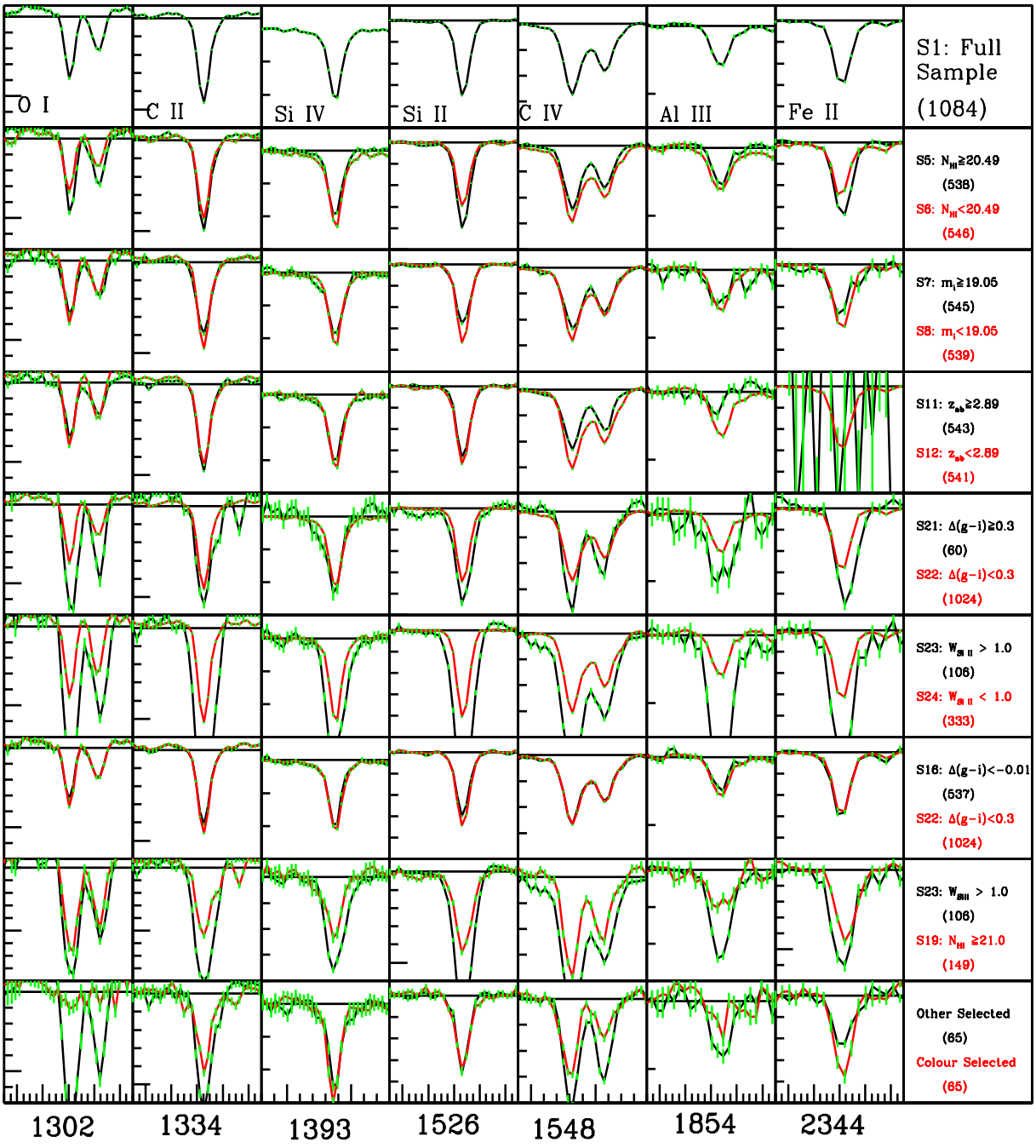

Figure 9. Comparison of several absorption lines in the composite spectra of a number of subsamples, defined in Table 1, constructed on the basis of absorber and QSO properties. The lines for the full sample are plotted in the top panel. Each row shows different lines in the composite spectra of the same two subsamples (one in red and the other in black), which are detailed in the last column of each row. Each column contains lines of the same species, indicated in the top row of that column, the wavelength of which is indicated below each column. One σ errors in the flux of the composite spectra are shown in green for each pixel. Scales are identical for all rows of a given column, except for the second from bottom panel, for which y axis scale goes to smaller values because of the stronger lines for the subsamples plotted in that row. The tick marks on the y axis are 0.1 units apart. The x axis spans 10 Å in all columns.

Table 4. Equivalent widths in mÅ for metal absorption features in the absorber rest frame in sample S1

Wavelength	Species	Sample S1	1(Y06)
1302.17	O I	413±14	
1304.37	Si II	266±14	
1334.53	C II	575±9	
1370.13	Ni II	47±5	
1393.32	Si IV	300±7	
1402.77	Si IV	230±7	
1526.71	Si II	447±4	383±10
1548.20	C IV	511±5	839±10
1550.78	C IV	300±21	580±9
1608.45	Fe II	227±4	
1656.93	C I	<12	19±4
1670.79	Al II	458±4	471±6
1709.60	Ni II	49±5	22±5
1741.55	Ni II	16±5	28±4
1751.92	Ni II	28±4	< 11
1808.00	Si II	51±2	68±5
1827.94	Mg I	< 7	<5
1854.72	Al III	107±3	183±4
1862.79	Al III	47±2	112±4
2026.48	Mg I+Zn II	33±5	40±4
2056.26	Cr II	26±3	39±4
2062.24	Cr II+Zn II	27±4	48±4
2066.16	Cr II	< 8	14±4
2249.88	Fe II	32±6	35±4
2260.78	Fe II	38±4	46±4
2344.21	Fe II	462±8	550±4
2367.59	Fe II	< 15	< 4
2374.46	Fe II	245±11	298±4
2382.77	Fe II	753±9	761±4
2576.88	Mn II	36±8	54±4
2586.65	Fe II	491±16	509±4
2594.50	Mn II	< 27	50±4
2600.17	Fe II	724±13	783±4
2606.46	Mn II	< 16	26±4
2796.35	Mg II[a]	1698±80	1432±4
2803.53	Mg II	836±73	1261±4

a: Only 22 systems have Mg II inside SDSS spectra

Table 5. Abundances as obtained from weakest lines

Sample	[Si/H]	[Cr/H]	[Mn/H]	[Fe/H]	[Ni/H]	[Zn/H]
S1	-1.29	-1.49	-1.99	-1.63	-1.35	-1.38

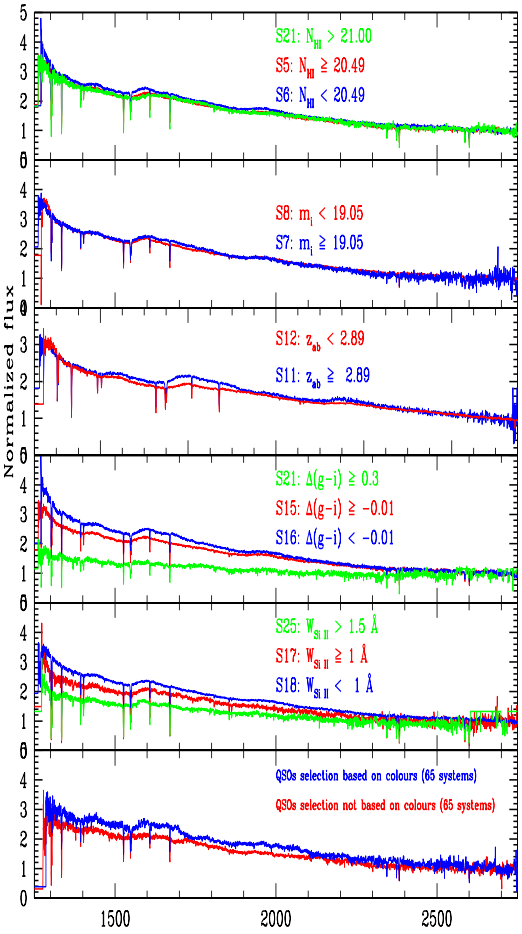

Figure 7. The geometric mean composite spectra of five sets of subsamples are plotted in the top five panels. The spectra are normalized at the long wavelength end. The subsamples are detailed in the legends. The scales along the x axis are the same for all panels except for the third panel where it goes from 1250-2350 Å as the low redshift composite spectra does not extend beyond that. The dust content is most clearly correlated with Si IIλ1526 equivalent width and $\Delta(g-i)$. In the bottom panel we have plotted the composites for DLAs along the lines of sight to colour selected QSOs (CS65) and along the lines of sight to QSOs not selected on the basis of colour (NCS65). The latter sample is more reddened compared to the colour selected sample. Note that both samples match in emission redshift and i magnitude distribution.

magnitude limited surveys and/or are too reddened to be included in the colour selected samples. Even though no evidence for this is found from studies of radio selected samples of QSOs (e.g. Ellison et al. 2001; Akerman et al. 2005; Jorgenson et al. 2006), it may be worth noting that a few of such QSOs have been observed by SDSS through other means of selection (see e.g. Noterdaeme et al.2009a) and have higher dust content and higher abundances. The SDSS data base would thus have very few of such systems. Ménard et al. (2008) have shown that the fraction of missed absorbers rises from 1 to 50% with increase in Mg II rest equivalent width from 1 to 6 Å.

We find a significantly higher dust content in DLAs along the lines of sight to SDSS QSOs that have not been selected on the basis of colours. Though the difference in the dust content of the two samples split by method of selection is not large, the finding is consistent with the expectations that dusty QSOs might be missed in SDSS due to colour selection bias. Therefore, the fraction of DLAs we find containing dust in the SDSS (∼10%) may be considered a lower-limit with respect to the global sample.

A larger survey of high-z QSOs selected without regard to optical colors is needed to more accurately measure the fraction of dusty DLAs at these redshifts. A substantial fraction of the z>2.2 quasars now being observed by the SDSS-III Baryon Oscillation Spectroscopic Survey have been targeted by alternate methods (Ross et al. 2011). These spectra may provide the necessary statistics to better explore the dust content of DLAs at high-z.

Should the small fraction of dusty DLAs hold in a less-biased

sample, one might speculate that the dust grain sizes may be different (larger) at high redshifts than those at lower redshifts. If the grains are large, there is no selective extinction at wavelengths below about 1/6 the smallest grain size in a mix which can explain the absence of reddening. The distribution of grain sizes and the extinction curve may then be changing with cosmic time. Examples of such flat extinction curves exist in the Galaxy, when $R_V = 5$ instead of the normal value of three (e.g. Mathis 1990). We reserve these conclusions for future work.

ACKNOWLEDGMENTS

PK thanks the Council of Scientific and Industrial Research, India for financial support.

Funding for the creation and distribution of the SDSS Archive has been provided by the Alfred P. Sloan Foundation, the Participating Institutions, the National Aeronautics and Space Administration, the National Science Foundation, the U.S. Department of Energy, the Japanese Monbukagakusho, and the Max Planck Society. The SDSS Web site is http://www.sdss.org/.

The SDSS is managed by the Astrophysical Research Consortium (ARC) for the Participating Institutions. The Participating Institutions are The University of Chicago, Fermilab, the Institute for Advanced Study, the Japan Participation Group, The Johns Hopkins University, the Korean Scientist Group, Los Alamos National Laboratory, the Max-Planck-Institute for Astronomy (MPIA), the Max-Planck-Institute for Astrophysics (MPA), New Mexico State University, University of Pittsburgh, University of Portsmouth, Princeton University, the United States Naval Observatory, and the University of Washington.

REFERENCES

Akeramn, C. J., Ellison, S. L., Pettini, M. & Steidel, C. C. 2005, A&A, 440, 499
Diplas, A. & Savage, B. D., 1994, ApJ, 427, 274
Eliasdottir, A. et al. 2009, ApJ, 697, 1725
Ellison, S. L., Yan, L., Hook, I. L., Pettini, M., Wall, J. V. & Shaver, P. 2001, A&A, 379, 393
Ellison, S. L., Hall, P. B., Lira, P. 2005, AJ, 130, 1345
Frank, S. & Péroux, C. 2010, MNRAS, 406, 2235
Gibson, R. R. et al. 2009, ApJ, 692, 758
Hollenbach D. J. & Salpeter E. E. 1970, ApJ, 163, 155
Hopkins P. F. et al. 2004, AJ, 128, 1112
Jiang, P., Ge, J., Prochaska, J. X., Kulkarni, V. P., Lu, H. L. & Zhou, H. Y., 2010, ApJ, 720, 328
Jorgenson, R. A., Wolfe, A. M., Prochaska, J. X., Lu, L., Howk, J. C.; Cooke, J., Gawiser, E. & Gelino, D. M. 2006, ApJ, 646, 730
Khare et al. 2007, A&A, 464, 487
Mathis, J. S., 1990, ARAA, 28, 37
Ménard, B., Nestor, D., Turnshek, D., Quider, A., Richards, G., Chelouche, D. & Rao, S., 2008, MNRAS, 385, 1053
Murphy, M. T. & Liske, J. 2004, MNRAS, 354, 31
Nestor, D. G., Pettini, M., Hewett, P. C., Rao, S., Wild, V. 2008, MNRAS, 390, 1670
Noterdaeme, P., Ledoux, C., Petitjean, P. & Srianand, R. 2008, A&A, 481, 327
Noterdaeme, P., Ledoux, C., Srianand, R., Petitjean, P. & Lopez, S. 2009a, A&A, 503, 765
Noterdaeme, P., Petitjean, P., Ledoux, C. & Srianand, R. 2009b, A&A, 505, 1087
Pei, Y. C., Fall, S. M. & Bechtold, J. 1991, ApJ, 378, 6
Pei, Y. C., Fall, S. M. & Hauser, M. G. 1999, ApJ, 522, 604
Pettini, M., King, D. L., Smith, L. J., & Hunstead, R. W., 1997, ApJ, 478, 536
Rachford, B. L. et al. 2002, ApJ, 577, 221
Richards, G. T. et al. 2003. AJ, 126, 1131
Ross, N. P., et al. 2011, arXiv:1105.0606
Schneider, D. P. et al. 2010, AJ, 139, 2360
Shen, Y. et al. 2011, ApJS, 194, 45
Srianand, R., Noterdaeme, P., Ledoux, C. & Petitjean, P. 2008, A&A, 482, L39
Stoughton, C. et al., 2002. AJ, 123, 485
Tumlinson, J. et al., 2002. ApJ, 566, 857
Vanden Berk D. et al. 2008, ApJ, 679, 239
Wild, V. & Hewett, P. C. 2005, MNRAS, 361, L30
Wild, V., Hewett, P. C.& Pettini, M. 2006, MNRAS, 367, 211
Yip, C. W. et al. 2004, AJ, 128, 2603
York et al. 2006, MNRAS, 367, 945